Flux through lipid synthesis dictates bacterial cell size.

Stephen Vadia,[1] Jessica L. Tse[2], Jue D. Wang[2] and Petra Anne Levin[1]*

[1]Department of Biology, Washington University in St. Louis, St. Louis, MO 63130, USA

[2]Department of Bacteriology, University of Wisconsin-Madison, Madison, WI 53706, USA.

*Correspondence: plevin@wustl.edu

Abstract

Nutrients—and by extension biosynthetic capacity—positively impact cell size in organisms throughout the tree of life. In bacteria, cell size is reduced three-fold in response to nutrient starvation or accumulation of the alarmone ppGpp, a global inhibitor of biosynthesis. However, whether biosynthetic capacity as a whole determines cell size or if particular anabolic pathways are more important than others remains an open question. Utilizing a top-down approach, here we identify flux through lipid synthesis as the primary biosynthetic determinant of *Escherichia coli* cell size. Altering flux through lipid synthesis recapitulated the impact of altering nutrients on cell size and morphology, while defects in other biosynthetic pathways either did not impact size or altered size in a lipid-dependent manner. Together our findings support a model in which lipid availability dictates cell envelope capacity and ppGpp functions as a linchpin linking surface area expansion with cytoplasmic volume to maintain cellular integrity.

Introduction

Cell size control is a fundamental aspect of biology. In multicellular organisms differences in cell size frequently dictate developmental fate, and defects in cell size are associated with cancer and other disease states (Ginzberg et al., 2015). In single celled organisms defects in cell size can be catastrophic, leading to failures in chromosome partitioning, bisection of genomic material during cytokinesis, and cell death (Hill et al., 2013; Rowlett and Margolin, 2015; Weart et al., 2007).

With the exception of asymmetric division and the formation of syncytia, cell size is dictated by two parameters: growth rate and cell cycle progression. Assuming growth rate remains constant, increasing the rate of cell cycle progression results in reductions in cell size. Conversely, maintaining the rate of cell cycle progression but increasing growth rate results in increases in cell size. Balancing these two parameters ensures cell size is maintained, an idea supported by the recent discovery that bacterial cells cultured under steady state conditions add a constant volume (Δ) prior to division regardless of their size at birth (Amir, 2014; Campos et al., 2014; Iyer-Biswas et al., 2014; Taheri-Araghi et al., 2015). Follow-up work indicates that deviations in birth size between *E. coli* cells in a clonal population are a consequence of stochastic differences in growth rate (Wallden et al., 2016).

Research on cell size homeostasis has historically focused on the role of the cell cycle. Most famously, the *wee1* kinase from *Schizosaccharomyces pombe* influences the timing of mitosis to maintain cell size, a function conserved in its many eukaryotic homologs (Kellogg, 2003; Wood and Nurse, 2015). In bacteria including the evolutionarily distant model organisms *Escherichia coli* and *Bacillus subtilis*, cell size is coupled with carbon availability in part via the UDP-glucose-dependent activation of a division inhibitor that delays the onset of cytokinesis to

increase cell length (Hill et al., 2013; Weart et al., 2007). Growth-dependent accumulation of the DNA replication initiation factor DnaA has also been implicated in cell size homeostasis under steady-state conditions through its impact on the timing and frequency of replication initiation (Lobner-Olesen et al., 1989; Wallden et al., 2016).

Although it has received considerably less attention, several lines of evidence support the idea that biosynthetic capacity, a product of nutrient availability, also serves as a primary determinant of cell size. Most important among these is the positive correlation between nutrient availability and cell size that exists throughout the tree of life. Drosophila cell and body size scale with nutrients, as does the size of baker's yeast, *Saccharomyces cerevisiae*, and fission yeast, *Schizosaccharomyces pombe* (Davie and Petersen, 2012; Edgar, 2006). The relationship between cell size, nutrient availability, and growth rate is linear in *Salmonella*, *E. coli* and *B. subtilis*. In all three bacterial species, organisms cultured under nutrient-rich conditions are up to three times the volume of those cultured under nutrient-poor conditions, a size increase too great to be accounted for solely by UDP-glucose-dependent division inhibition (Hill et al., 2013; Pierucci, 1978; Sargent, 1975; Schaechter et al., 1958; Weart et al., 2007). Significantly, Δ, the volume of material that *E. coli* cells add each generation, increases in carbon rich conditions and decreases in carbon poor conditions, suggesting that changes in biosynthetic capacity shift the balance between growth rate and the rate of cell cycle progression (Campos et al., 2014; Taheri-Araghi et al., 2015).

In further support of biosynthetic capacity as an important determinant of cell size, accumulation of guanosine tetraphosphate (ppGpp), an inhibitor of a host of biosynthetic pathways, is negatively correlated with bacterial size. Increasing intracellular ppGpp concentration directly via overexpression of the ppGpp synthase RelA reduces the growth rate

and size of *E. coli* cultured in nutrient rich medium (Schreiber et al., 1995; Tedin and Bremer, 1992). Indirectly stimulating ppGpp accumulation via amino acid starvation or by limiting fatty acid synthesis, similarly leads to reductions in both growth rate and cell size (Tehranchi et al., 2010; Yao et al., 2012a).

Because ppGpp is a global regulator of biosynthesis in bacteria (Liu et al., 2015), however, it is impossible to know if ppGpp-dependent reductions in size are the result of changes in biosynthetic capacity as a whole, or if particular anabolic pathways play a more important role than others in modulating cell size. Thus, while amino acid starvation or limitations in fatty acid synthesis may directly impact cell size, it is equally likely that they are affecting size indirectly via increases in ppGpp concentration and the concomitant global down-regulation of biosynthetic capacity. This precise conundrum was noted by Yao *et al*. in their 2012 paper reporting a reduction in *E. coli* size associated with defects in a gene required for an early step in fatty acid synthesis (Yao et al., 2012a).

To illuminate the role of biosynthetic capacity in cell size control, we employed a top-down strategy to assess the contribution of three major anabolic pathways to *E. coli* morphology and growth rate. Our findings unequivocally and for the first time establish flux through lipid synthesis as a primary, ppGpp-independent determinant of bacterial cell size. Not only did increasing flux through lipid synthesis lead to dramatic ppGpp-independent increases in cell size, defects in other major pathways impacted by ppGpp had either no significant impact on size (RNA synthesis) or reduced size in a lipid-dependent manner (protein synthesis). Importantly, increases in flux through lipid synthesis significantly increased both cell length and width, almost perfectly recapitulating the effect of nutrients on cell morphology in both magnitude and kind. The positive relationship between lipid synthesis and cell width distinguishes it from cell

cycle progression, changes in which almost exclusively impact cell length (Harris and Theriot, 2016; Pritchard et al., 1978; Young, 2010).

Taken together our findings support a novel "outside-in" model in which size is dictated by the capacity of the cell envelope, which is itself a product of nutrient-dependent changes in lipid synthesis and availability. This lipid-centric view has implications for essentially all aspects of bacterial physiology that are sensitive to changes in nutrient availability. In particular, changes in cell envelope biogenesis must be coordinated with synthesis of cytoplasmic material to ensure that cytoplasmic volume does not exceed plasma membrane capacity. Our data suggest that ppGpp plays a central role in this process, tethering lipid synthesis to cytoplasmic aspects of anabolic metabolism to preserve cell envelope integrity in the face of a rapidly changing nutritional landscape.

Results

RNA, protein and fatty acid synthesis differentially impact cell size

To identify the major biosynthetic pathways underlying cell size control, we utilized a top-down approach, modifying the growth rate of *E. coli* cultured in nutrient-rich medium (LB + 0.2% glucose; LB-glc) with subinhibitory concentrations of antibiotics targeting RNA (rifampicin), protein (chloramphenicol), and fatty acid (cerulenin) synthesis. Synthesis of RNA, protein, and fatty acids is nutrient-dependent, and all three pathways are down-regulated in response to increases in ppGpp levels, either directly (RNA), or indirectly (protein and fatty acid synthesis) (Heath et al., 1994; Podkovyrov and Larson, 1996; Schreiber et al., 1991; Svitil et al., 1993). In light of the well-documented association between defects in DNA replication and activation of both SOS-dependent and -independent modes of division inhibition, we elected not to investigate the impact of reductions in DNA synthesis on size (Arjes et al., 2014; Cambridge et al., 2014; D'Ari and Huisman, 1983; Huisman and D'Ari, 1981; Huisman et al., 1984). We similarly chose not to examine the consequence of defects in cell wall biogenesis on cell size, as treatment with antibiotics targeting peptidoglycan synthesis disproportionally effect cell division, leading to extensive filamentation even at low concentrations (Burke et al., 2013; Fredborg et al., 2015; Yao et al., 2012b).

To assess the impact of limitations in RNA, protein, or fatty acid synthesis on cell size, BH330 cells [MG1655 P_{lac}::*gfp-ftsZ* (*bla*) (Hale and de Boer, 1999)] were first cultured to early log phase in LB-glc, then back-diluted to an OD_{600} of 0.005 into fresh medium with subinhibitory concentrations of the appropriate antibiotic and 1 mM IPTG to induce expression from P_{lac}-*gfp-ftsZ*, and cultured for ~ 6 generations (OD_{600} ~ 0.3) prior to being fixed, imaged, and measured. Notably, we did not detect any significant differences in growth rate or cell size if

chloramphenicol or cerulenin treated cells were back-diluted a second time into fresh medium and cultured for an additional 6 generations at the same drug concentration. However, in the presence of the highest concentration of rifampicin (6 μg/ml), cells were unable to reach a substantial OD_{600} upon back-dilution, suggesting that robust transcription is a requirement for exit from early log growth (Table S3). As a benchmark, we also modified growth by culturing cells in six different media: LB-glc, LB, and AB minimal medium ± 0.5% casamino acids with 0.2% glucose or 0.4% succinate (AB-caa-glc, AB-caa-succ, AB-glc, AB-succ). Measurements from ≥400 cells from ≥3 biological replicates were used to generate single data points and histograms for each condition. Cell length and width analysis was performed using the Image J plug-in, Coli-Inspector (Vischer et al., 2015).

Consistent with previous studies, reductions in nutrient availability led to decreases in both growth rate and size (Figures 1 and S1) (Pierucci, 1978; Sargent, 1975; Schaechter et al., 1958). *E. coli* cultured in LB-glc grew to a mean length (*l*) of 3.76 μm, mean width (*w*) of 1.07 μm and mean square area (*a*) of 4.11 μm^2, while those cultured in minimal succinate, the poorest carbon source, were 48% smaller by area (a = 2.07 μm^2) in addition to being shorter and thinner (l =2.63 μm, w = 0.79 μm).

Of the three antibiotics, only cerulenin, an inhibitor of the β-ketoacyl-ACP synthase I, FabB, reduced both growth rate and size in a manner that closely mimicked effects of nutrient limitation (Figures 1 and S1A; For reference the carbon curve is depicted as a black line in the plots of cell size versus growth rate following antibiotic treatment). In the presence of 70 μg/ml of cerulenin, cells cultured in LB-glc exhibited a growth rate and size similar to that of untreated cells cultured in AB-caa-glc (LB-glc + cer: mean mass doubling time/hour (τ) = 1.36 d/h, l = 2.93 μm, w = 0.95 μm, a = 2.88 μm^2; AB -caa-glc: τ = 1.4 d/h, l = 2.56 μm, w = 0.96 μm, a =

2.44 μm^2). This reduction in size is similar to that previously reported for cerulenin treated cells (Yao et al., 2012a). While treatment with between 0.5 μg/ml and 1.5 μg/ml of chloramphenicol reduced cell length to 3.14 μm, width remained essentially constant (~1.0 to 1.1 μm). Inhibiting transcription with rifampicin dramatically reduced growth rate but did not reduce cell size at even the highest concentration of antibiotic (6 μg/ml). The 10% reduction we observed in chloramphenicol-treated cell size is similar to that previously reported by the Hwa and Theriot labs (Basan et al., 2015a; Basan et al., 2015b; Harris and Theriot, 2016). The size and growth rate of BH330 cells cultured under different nutrient conditions were essentially identical to the size and growth rate of the wild type MG1655 parental strain cultured under the same conditions, indicating that expression of P_{lac}::*gfp-ftsZ* did not significantly impact cell growth or physiology (Figure S1B).

While the three antibiotics differentially impacted cell size, none of them significantly disrupted the relationship between growth rate and cell cycle progression. Assembly of the tubulin-like protein FtsZ into a ring-like structure at the nascent division site is an essential phase of cytokinesis in bacteria. The FtsZ ring serves as a framework for assembly of the division machinery and is a useful marker for cell cycle progression (Adams and Errington, 2009; den Blaauwen et al., 1999). While 80-90% of cells cultured in nutrient rich conditions have FtsZ rings, rings are visible in only 40-50% of their slow growing counterparts cultured in nutrient poor medium, consistent with a reduced rate of cell cycle progression (den Blaauwen et al., 1999; Weart and Levin, 2003).

Taking advantage of the P_{lac}::*gfp-ftsZ* construct in BH330 cells, we determined that the proportion of cells with distinct FtsZ rings (visualized as two parallel fluorescent spots at midcell, a band across the width of the cell, or as a single point in a constricting cell) remained

193 inversely proportional to mass doubling time, regardless of the method (nutrient depletion or
194 antibiotic treatment) used to reduce growth rate (Figure 1B). Although depressed relative to other
195 growth conditions - potentially due to reductions in expression of both native *ftsZ* and P_{lac}::*gfp-*
196 *ftsZ* - the frequency of FtsZ rings remained inversely proportional to mass doubling time in
197 rifampicin treated cells (Figure 1B).
198
199 **Cells lacking *fabH* adjust their width in response to nutrient availability**
200 The dose-dependent effect of cerulenin on cell size suggests a proportional relationship
201 between size and flux through fatty acid synthesis. To test this idea we took advantage of
202 previous work from the Ruiz laboratory, indicating that *E. coli* cells defective in *fabH*, encoding
203 the enzyme responsible for catalyzing the initiating condensation reaction in fatty acid synthesis
204 (β-ketoacyl-acyl carrier protein synthase III), are viable due to the presence of an as yet
205 uncharacterized bypass mechanism that permits growth in the absence of what was previously
206 assumed to be an essential gene (Yao et al., 2012a).
207 Reasoning that if size is in fact proportional to flux through fatty acid synthesis, as our
208 cerulenin data suggest, the linear relationship between nutrient availability and cell size should
209 be partially retained in a *fabH* mutant due to the presence of the putative bypass mechanism. In
210 support of a direct relationship between flux through fatty acid synthesis and cell size, *fabH*
211 mutants increased in size in response to increases in carbon availability, although not to the same
212 extent or in the same manner as wild-type *E. coli*. *fabH* mutants cultured in the poorest medium
213 (AB-succ) (τ = 0.74 d/h), had a mean square area (*a*) of 2.04 μm^2, those cultured in intermediate
214 conditions, AB-caa-glc (τ = 1.28 d/h) and AB-caa-succ (τ = 1.00 d/h), both had mean square
215 areas of 2.15 μm^2, and those cultured in the richest medium, LB-glc (τ = 1.34 d/h), a mean

square area of 2.54 μm^2 (Figure 1C). Interestingly, length remained relatively constant across growth conditions (LB-glc *l* = 2.42 μm; AB-succ *l* = 2.45 μm) but width changed substantially (LB-glc *w* = 1.05 μm; AB-succ *w* = 0.83).

We note that our finding that *fabH* mutants maintain a positive relationship between size and nutrient availability runs counter to those of Yao *et al*., who reported that *fabH* mutants are compromised in their ability to modulate size in response to nutrients. In their hands *fabH* mutant length and width were essentially identical in rich or minimal media (LB and M63 minimal salts + 0.2% glucose) [Table 4 (Yao et al., 2012a)]. We attribute this discrepancy to the broad range of carbon sources we employed, which in turn allowed for a broader range in flux through fatty acid synthesis.

Protein synthesis-dependent changes in cell size are lipid-dependent

Our observation that treatment with chloramphenicol resulted in a modest but significant reduction in cell size (Figures 1 and S1), suggested that protein synthesis is either a direct determinant of cell size or, alternatively, that it indirectly impacts size via secondary effects on fatty acid synthesis. To resolve this issue, we took advantage of *E. coli*'s ability to incorporate exogenous long chain fatty acids, such as oleic acid, into its plasma membrane (Black and DiRusso, 2003; Cronan, 2014). Briefly, we cultured BH330 cells in LB-glc with 1.5 μg/ml of chloramphenicol, in the presence or absence of exogenous oleic acid. As controls we also added oleic acid to cells cultured in the presence of 70 μg/ml cerulenin and to untreated cells.

Supporting a primary role for lipids in cell size control, the addition of exogenous long chain fatty acids reversed both the growth rate and size defect of cerulenin and chloramphenicol-treated cells (Figure 2A and B; Table S4). As expected, cerulenin-treated cells increased

239 substantially in size and growth rate in the presence of 10 μg/ml of oleic acid. Strikingly, and in
240 agreement with the idea that chloramphenicol impacts size indirectly via reductions in cellular
241 levels of key enzymes involved in fatty acid synthesis, exogenous oleic acid partially corrected
242 the growth rate and cell size defects of chloramphenicol-treated cells, which were 10% larger
243 and grew 16% faster after 5-6 generations in the presence of 10 μg/ml oleic acid than in its
244 absence (+ oleic acid: $a = 3.70 \pm 0.16$ μm^2, $\tau = 2.09$ d/h; - oleic acid: $a = 3.35 \pm 0.15$ μm^2 and τ
245 = 1.82 d/h) (Figure 2B). Cell width remained essentially unchanged in the presence and absence
246 of oleic acid ($w = 1.10 \pm 0.03$). Oleic acid had no impact on bacteria in the absence of antibiotics,
247 suggesting they were at steady state with regard to synthesis and incorporation of fatty acids
248 (Figure S1C).
249
250 **Cell size scales with lipid synthesis independent of ppGpp**
251 A significant limitation of the preceding experiments as well as previous work
252 investigating the relationship between fatty acid synthesis and cell size, has been the use of
253 mutations or antibiotics that interfere with the earliest steps in fatty acid synthesis and lead to a
254 four- to five-fold increase in intracellular ppGpp levels due to reductions in SpoT hydrolase
255 activity (Battesti and Bouveret, 2006; Seyfzadeh et al., 1993). ppGpp in turn down-regulates
256 transcription of a host of genes including those encoding ribosomal RNAs, and enzymes
257 essential for fatty acid and phospholipid synthesis (Heath et al., 1994; Liu et al., 2015). Inhibiting
258 early steps in fatty acid biosynthesis may thus impact size indirectly, via a ppGpp-dependent but
259 fatty acid-independent mechanism.
260 To clarify the relationship between lipid synthesis and cell size we therefore sought to
261 manipulate lipid pools through alternative means: increasing synthesis of the entirety of genes

required for fatty acid synthesis via induction of the transcriptional activator FadR. FadR functions as both a transcriptional activator, driving expression of genes required for fatty acid synthesis, and as a repressor, dampening expression of genes involved in the breakdown of fatty acids through beta-oxidation in response to nutritional stress (My et al., 2013). Overproduction of FadR leads to the bulk accumulation of long chain fatty acids in wild-type cells (Zhang et al., 2012). To overproduce FadR, we employed plasmid *pE8k-fadR* (hereafter *pFadR*) encoding an inducible/repressible allele of *fadR* (the kind gift of Dr. Fuzhong Zhang).

Consistent with a positive relationship between fatty acid synthesis and cell size, induction of *fadR* led to a dose-dependent increase in cell size (Figure 3A and B; Table S5). Even in the absence of inducer, the mean square area of MG1655 cells bearing *pFadR* was ~ 20% higher than MG1655 without the plasmid (*pFadR* a = 4.60 μm^2; MG1655 a = 3.77 μm^2) exhibiting increases in both length and width (*pFadR* l = 3.99 μm, w = 1.14 μm; MG1655 l = 3.53 μm, w = 1.07 μm). At 10μM IPTG, the highest concentration of inducer, *pFadR* cells were nearly twice the size of those from the parental strain (*pFadR* 10μM IPTG a= 7.15 μm^2 , l = 5.67, w = 1.23). Importantly, overproduction of FadR dramatically increased not only average cell size, but also shifted the entire cell size distribution towards larger cells (Figure 3C).

Intriguingly, induction of *fadR* inverted the relationship between size and growth rate. While *pFadR* cells were approximately twice as large as the parental strain in the presence of maximal amounts of inducer, they grew nearly 30% slower (*pFadR* 10 μM IPTG τ = 2.09 d/h; MG1655 τ = 2.88 d/h) (Table S5). This reduction in growth rate is most likely a consequence of reductions in other aspects of anabolic metabolism due to increased carbon flux through lipid synthesis. Importantly, induction of *fadR* did not significantly impact the ratio of ppGpp to GTP,

284 consistent with a model in which fatty acid synthesis influences size independent of the alarmone
285 (Figure S2A).
286
287 **Flux through lipid synthesis impacts cell size downstream of ppGpp**
288 To confirm if lipid synthesis impacts size downstream of ppGpp as our *fadR*
289 overexpression data suggested, we next assessed the ability of FadR to overcome the size defect
290 associated with increases in intracellular ppGpp levels. ppGpp together with the RNA
291 polymerase binding protein DksA, inhibits transcription of the genes required for fatty acid
292 synthesis as well as *fadR* (My et al., 2013). If ppGpp mediates size through down-regulation of
293 fatty acid synthesis, overproduction of FadR should increase the size of cells overexpressing
294 ppGpp. Alternatively, if ppGpp impacts size downstream of fatty acid synthesis, overproduction
295 of FadR should have little impact on the size of cells overexpressing ppGpp.
296 For these experiments we utilized a plasmid (*pALS10* hereafter *pRelA;* the kind gift of Dr.
297 Charles Rock) encoding a copy of the ppGpp synthase *relA* under the control of an IPTG
298 inducible promoter (Svitil et al., 1993). Consistent with previous studies, ppGpp had a negative
299 impact on cell size. In the absence of inducer, *pRelA* cells were on average 25% smaller than the
300 MG1655 parental strain (*pRelA* a = 2.94 μm^2; l = 3.08 μm, w = 0.96 μm) (Figure 4A; Table S5).
301 The addition of 10μM IPTG further reduced *pRelA* cells to ~55% of wild-type size (*pRelA* + 10
302 μM IPTG a = 2.20 μm^2; l = 2.34 μm, w = 0.94 μm). *pRelA* also led to a marked increase in mass
303 doubling time, consistent with reports indicating that even modest increases in intracellular
304 ppGpp levels have a strong, negative impact on growth (*pRelA* τ = 2.09; *pRelA* + 10 μM IPTG
305 τ = 1.46; MG1655 τ = 2.64) (Sarubbi et al., 1988).

306 To ascertain if lipid synthesis impacts size downstream of ppGpp, we next generated a
307 strain carrying both *pRelA* and *pFadR*. Because *relA* and *fadR* are both under the control of an
308 IPTG-inducible promoter, FadR and ppGpp levels should both rise in the presence of IPTG.
309 Consistent with a model in which ppGpp impacts size directly via down-regulation of fatty acid
310 synthesis, cells harboring both *pRelA* and *pFadR*, were larger than cells carrying *pRelA* alone
311 regardless of the presence of inducer (*pRelA*/*pFadR* - inducer a = 4.15 μm^2; l = 3.89 μm, w
312 =1.07 μm; *pRelA*/*pFadR* 10 μM IPTG a = 4.76 μm^2; l = 4.29 μm, w = 1.09 μm) (Figure 4A;
313 Table S5). Co-induction of *fadR* and *relA* did not substantially alter the growth rate of
314 *pRelA*/*pFadR* cells (*pRelA*/*pFadR* – inducer τ = 1.92 d/h; *pRelA*/*pFadR* + 10 μM IPTG τ = 1.71
315 d/h), nor did it significantly impact the ppGpp to GTP ratio (Figure S2B).
316
317 **The linear relationship between cell size and nutrient availability is retained in the absence**
318 **of ppGpp**
319 If flux through fatty acid synthesis is indeed a primary determinant of cell size as the
320 above data suggest, *E. coli* should retain a linear relationship between size and nutrient
321 availability regardless of the presence of ppGpp. To test this possibility, we examined the growth
322 rate and size of *E. coli* defective in ppGpp synthesis (ppGpp^0) cultured under four different
323 carbon conditions (LB-glc, LB, AB-caa-glc and AB-caa-succ). [Due to multiple auxotrophies it
324 is not possible to culture ppGpp^0 cells in minimal medium without amino acid supplementation
325 (Xiao et al., 1991)]. The ppGpp^0 strain PAL3540 encodes loss-of-function mutations in both *relA*
326 and *spoT* (MG1655 *spoT*::*cat*, *relA*::*kan*), and is thus unable to synthesize the alarmone.
327 Mean square area remained inversely proportional to growth rate in ppGpp^0 cells,
328 indicating that size and nutrient availability remain coupled in the absence of ppGpp (Figure 4B;

Table S2). Larger than congenic wild-type cells — potentially due to "free running" fatty acid synthesis in the absence of the alarmone — ppGpp^0 mutants cultured in LB-glc and LB had mean square areas of a = 6.25 μm^2 (l = 4.46 μm, w = 1.16 μm, τ = 1.92 d/h) and 7.23 μm^2 (l = 6.19 μm, w = 1.14 μm , τ = 1.68 d/h) respectively, while those cultured in AB-caa-glc had a mean square area of 3.01 μm^2 (l = 2.98 μm, w = 0.97 μm, τ = 1.12 d/h) and those in AB-caa-succ a mean square area of 3.46 μm^2 (l = 3.45 μm, w = 1.00 μm , τ = 0.96 d/h) (Figure 4B; Table S2). While we observed some extremely long ppGpp^0 cells during growth in LB and LB-glc, such cells were absent during growth in minimal medium (Figure S3).

ppGpp is required to maintain cell envelope integrity in the absence of fatty acid synthesis

Defects in fatty acid synthesis are incompatible with reductions in ppGpp synthesis (Yao et al., 2012a). Although not essential in a wild-type background, *fabH* is absolutely required in strains that are defective in one or both ppGpp synthases, RelA and SpoT (Yao et al., 2012a). Given this relationship, we wondered if an increase in intracellular [ppGpp] in response to defects in fatty acid synthesis might be protective, down-regulating other aspects of biosynthetic capacity to ensure that accumulation of cytoplasmic material does not exceed the capacity of the plasma membrane. To test this possibility, we examined the viability and membrane integrity of wild-type and ppGpp^0 cells cultured in the presence of 500 μg/ml cerulenin (~5 times the MIC for wild-type cells).

Supporting a protective role for the alarmone, ppGpp^0 cells were four orders of magnitude more sensitive to treatment with the fatty acid inhibitor cerulenin than their wild-type counterparts (Figure 5A). Cerulenin is generally viewed as bacteriostatic antibiotic, blocking synthesis of fatty acids without significantly impairing viability. Consistent with bacteriostatic

activity, the plating efficiency of wild-type *E. coli* (MG1655) cells was largely unchanged after 4 hours of growth in the presence of 500 µg/ml cerulenin. In contrast, cerulenin treatment of ppGpp^0 cells was bactericidal with plating efficiency dropping 10,000-fold over the course of 2.5 hours (Figure 5A).

To assess the impact of cerulenin on cell envelope integrity, we visualized uptake of the dye, propidium iodide (PI), in wild-type and ppGpp^0 cells in real time following cerulenin addition. PI is a nucleic acid intercalating agent that is unable to efficiently cross intact cellular membranes. When bound to nucleic acids, the fluorescence intensity of PI increases 20 to 30-fold. Due to its large size, however, PI requires pores of at least 2 nm to enter cells and bind to nucleic acid, a size generally incompatible with viability. PI fluorescence is thus a good indicator of loss of membrane integrity (Arndt-Jovin and Jovin, 1989; Bowman et al., 2010; Golzio et al., 2002).

PI staining strongly supports the idea that ppGpp accumulation preserves membrane integrity in response to inhibition of fatty acid synthesis through down regulation of other aspects of macromolecular synthesis (Figure 5B and C). The entirety of the ppGpp^0 population exhibited bright red fluorescence indicative of a severe loss of membrane integrity three hours after the addition of 500 µg/ml of cerulenin (Figure 5C). In contrast, only a few PI-positive cells were visible in wild-type cells at the same time point. Calculation of mean fluorescence intensity suggests that wild-type cells were largely impermeable to the dye: 28 AU/cell (AU= arbitrary units) 30 minutes after the addition of drug rising to only 51 AU/cell two hours after the addition of drug. In contrast, ppGpp^0 cells readily incorporated PI after the addition of cerulenin The mean fluorescence intensity of ppGpp^0 mutants reached ~50 AU/cell within 60 minutes of cerulenin treatment and rose to 450AU/cell at 2.5 hours (Figure 5B).

Discussion

This study firmly establishes lipid availability, and by extension cell membrane capacity, as a primary biosynthetic determinant of *E. coli* cell size (Figure 6). Increasing lipid synthesis, via overproduction of the transcriptional activator FadR, led to dose-dependent increases in cell size, while inhibiting lipid synthesis led to dose-dependent reductions in cell size (Figures 1 and 3). The modest reduction in length resulting from treatment with the translation inhibitor chloramphenicol was abolished by the addition of oleic acid to the medium (Figure 2B), further reinforcing a direct link between cell size and lipid availability. Inhibiting transcription had no detectable impact on cell morphology.

A direct relationship between lipid synthesis and cell size provides a potential explanation for both the observation that bacterial cells add a constant volume (Δ) each generation under steady-state conditions as well as the strikingly linear relationship between nutrient availability and cell size. During balanced growth, a constant rate of flux through fatty acid synthesis coupled with a relatively invariant cell cycle clock translates into the addition of a constant volume of material in each generation. Shifting cells to carbon rich medium increases flux through fatty acid synthesis, transiently altering the balance between biosynthetic capacity and cell cycle progression until a new equilibrium is established albeit at a larger size (Δ). This model is supported both by data indicating that the rate of fatty acid synthesis is proportional to carbon availability (Davis et al., 2000; Li and Cronan, 1993) as well as Stephen Cooper's observation that *E. coli* immediately increases its growth rate upon a shift to nutrient rich medium but delays division until cells achieve a new, larger size (Cooper, 1969). In *E. coli*, lipids are effectively all directed to the membrane (Parsons and Rock, 2013). Changes in the pool

of lipids available for cell envelope biogenesis are thus expected to proportionally impact cell size.

Importantly, this study is the first to definitively place lipid synthesis downstream of ppGpp with regard to cell size. Inducing expression of the transcriptional activator of fatty acid synthesis, FadR, not only increased the size of wild-type cells, but also overcame the size defect associated with overproduction of the ppGpp synthase RelA (Figures 3 and 4A). Moreover, treatment with chloramphenicol, which mimics a "relaxed" (low ppGpp) state, reduced cell size in a lipid-dependent manner (Figure 2B). Cells defective in ppGpp production retained a linear relationship between size and nutrient availability, further reinforcing the idea that flux through lipid synthesis is a primary dictator of cell size independent of the alarmone (Figure 4B).

Changes in lipid synthesis mimic the impact of nutrients on cell size and morphology

Like nutrients, altering flux through fatty acid synthesis impacted both the length and width of *E. coli* cells (Figures 1 and 3, Tables S2, S3 and S5). In our hands *E. coli* cultured in nutrient poor medium were ~30% shorter and ~25% thinner than their counterparts cultured in nutrient rich medium (Figure 1; Table S2). Cells cultured in nutrient rich LB-glc with 70 μg/ml of cerulenin exhibited a 20% reduction in length and a 10% reduction in width, in total a 30% reduction in square area that rendered them essentially indistinguishable from their counterparts cultured in AB-caa-glc. Overproduction of FadR increased cell length by 60% and cell width by 15%, increasing square area ~2-fold, a morphological change proportional to that observed in wild-type *E. coli* cells shifted from AB-succ to LB-glc [Figure 1 (Carbon); Figure 4; Tables S2 and S5].

The significant impact of lipid synthesis on both cell length and cell width distinguishes it

421 from the relationship between cell cycle progression and cell size. Inhibiting divisome assembly
422 can dramatically increase cell length, however, cell width is largely unaffected and in some cases
423 may even be reduced (Harris and Theriot, 2016; Young, 2010). Delaying DNA replication
424 initiation by depleting DnaA similarly leads to significant increases in cell length but does not
425 detectably impact width (Pritchard et al., 1978).

426 **ppGpp: a master regulator coordinating lipid synthesis with other aspects of anabolic**
427 **metabolism to preserve cellular integrity**

428 A role for plasma membrane capacity as a primary determinant of cell size has far
429 reaching implications for essentially all major aspects of cellular physiology that are sensitive to
430 nutrient availability. Most obviously, lipid synthesis must be coordinated with synthesis of
431 cytoplasmic material—particularly DNA, RNA and protein—to link surface area expansion with
432 cytoplasmic volume and maintain cell envelope integrity. In this regard, our data suggest ppGpp
433 plays a critical role, ensuring that flux through fatty acid synthesis is coupled to other aspects of
434 biosynthetic capacity (Figures 5 and 6). In contrast to wild-type cells for which the addition of
435 the fatty acid synthesis inhibitor cerulenin was bacteriostatic, $ppGpp^0$ mutants exhibited a 10-
436 fold reduction in viability within 30 min of addition of cerulenin, and gradually became
437 permeable to propidium iodide (Figure 5). A role for ppGpp in coordinating fatty acid synthesis
438 with cytoplasmic aspects of biosynthetic capacity is consistent with the longstanding observation
439 that defects in ppGpp synthesis impair the ability of cells to respond to nutrient downshift
440 (Murray et al., 2003; Ross et al., 2013; Sarubbi et al., 1988).

441 Loss of cell envelope integrity may also be a consequence of defects in coordination
442 between lipid production and cell wall synthesis. Accumulation of ppGpp leads to down
443 regulation of enzymes required for peptidoglycan synthesis and reduces the rate of

444 diaminopimelic acid incorporation (Ishiguro and Ramey, 1976, 1978; Traxler et al., 2008). A
445 negative relationship between ppGpp accumulation and cell wall synthesis is consistent with
446 both our findings and the recent suggestion from Harris and Theriot that surface growth is
447 coordinated with cell volume via growth rate-dependent changes in accumulation of cell wall
448 precursors (Harris and Theriot, 2016). Independent of ppGpp, the reliance of peptidoglycan
449 synthesis on availability of the 55-carbon lipid carrier, undecaprenyl pyrophosphate, may render
450 it intrinsically dependent on flux through central carbon metabolism. In *B. subtilis* lipid
451 production is enhanced upon depletion of enzymes required for synthesis of peptidoglycan
452 precursors, suggesting the potential for a feedback loop coupling peptidoglycan and lipid
453 synthesis to one another (Mercier et al., 2013).
454 Although unlikely to directly impact cell envelope integrity, membrane synthesis must
455 also be synchronized with cell cycle progression to ensure the production of viable daughter
456 cells. ppGpp has previously been implicated in coordinating amino acid starvation with both
457 DNA replication and chromosome segregation. In *E. coli*, treatment with serine hydroxamate
458 results in ppGpp-dependent inhibition of replication elongation in addition to a reduction in cell
459 size (Tehranchi et al., 2010). ppGpp is also reported to interfere with chromosome segregation,
460 although the mechanism underlying this phenomenon in unclear (Ferullo and Lovett, 2008).
461 Induction of ppGpp upon inhibition of fatty acid synthesis serves an adaptive function for the
462 alphaproteobacterium *C. crescentus*, down-regulating production of both the global cell cycle
463 regulator CtrA as well as DnaA to prevent DNA replication in the absence of growth (Leslie et
464 al., 2015; Stott et al., 2015).
465

Beyond *E. coli*

It remains to be seen if lipid synthesis and plasma membrane capacity are widely conserved as a link between nutrient availability and cell size. Little is known about the relationship between fatty acid synthesis and ppGpp synthesis in the Gram-positive model bacterium *B. subtilis*. Moreover, many bacteria, including the pathogen *Mycobacterium tuberculosis*, store lipids in self-contained, cytoplasmic vacuoles. How lipid storage is balanced with cell envelope biogenesis in such organisms remains an open question. Further afield, the target of rapamycin (TOR) kinase, promotes the growth and proliferation of eukaryotic cells in response to increases in nutrient availability, including the presence of growth factors and other generally auspicious environmental conditions (Laplante and Sabatini, 2009; Loewith and Hall, 2011). While much of the literature has focused on the role of TOR in regulating protein synthesis, TOR has also been implicated in stimulating lipid synthesis, both for cell membrane and storage purposes (Laplante and Sabatini, 2009). It is thus of great interest to know whether the relationship between lipid pools and cell size that we observed in *E. coli*, holds true in eukaryotes, where fatty acid synthesis is restricted to the mitochondria.

Materials and Methods

Bacterial strains and culture conditions

E. coli strains and plasmids are listed in table S1. Standard techniques were employed for P1 vir transductions and other genetic manipulations. Cells were cultured in lysogeny broth (LB) + 0.2% glucose or AB minimal medium (Clark, 1967) supplemented with 10 μg/ml thiamine, 5 μg/ml thymidine and 0.5% casamino acids, 0.2% glucose or 0.4% succinate as indicated. Strains carrying plasmids were cultured with 100 μg/ml ampicillin or 50 μg/ml kanamycin as required. Cells were used for experimentation at early exponential growth phase (OD_{600} = 0.15-0.3) unless stated otherwise. To achieve balanced growth, cells were cultured at 37°C in the indicated medium from a single colony to early exponential phase with vigorous shaking (200 rpm). Cultures were then back-diluted into fresh medium to an OD_{600} of 0.005 and cultured to early exponential phase prior to being sampled and fixed for analysis. For experiments in minimal medium, cells were first cultured from a single colony overnight prior to being back-diluted into minimal medium to an OD_{600} of 0.005 and subjected to an additional round of growth and back-dilution as above. In experiments utilizing sub-inhibitory concentrations of rifampicin, chloramphenicol or cerulenin to inhibit RNA, protein or fatty acid synthesis, antibiotics were added when cultures were back-diluted. In experiments involving isopropyl β-D-1-thiogalactopyranoside (IPTG) or exogenous fatty acids, they were added along with antibiotics at the indicated concentrations. Mass doubling times were calculated from OD_{600} readings taken every 30 minutes using the online doubling time calculator, cell calculator++ (Roth, 2006). For experiments utilizing the $ppGpp^0$ strain, PAL3540 (MG1655 *relA*::*kan spoT*::*cat*), cells were plated on AB minimal medium + 0.2% glucose and LB agar to confirm that they had not

accumulated suppressor mutations that suppressed the auxotrophies associated with the absence of ppGpp.

Microscopy and image analysis

Images were acquired from samples on 1% agarose (in PBS) pads with an Olympus BX51 microscope equipped with a 100X Plan N (N.A. = 1.25) Ph3 objective (Olympus), X-Cite 120 LED light source (Lumen Dynamics), and an OrcaERG CCDcamera (Hammamatsu Photonics, Bridgewater, N.J.). Filter sets for fluorescence were purchased from Chroma Technology Corporation. Nikon Elements software (Nikon Instruments, Inc.) was used for image capture. Cells were fixed with 2.6% paraformaldehyde + 0.008% glutaraldehyde, and stained with the membrane stain FM 4-64$_{fx}$ (ThermoScientific) prior to imaging as described previously (Levin, 2002). Cell size was determined from phase contrast images with the ImageJ pulgin Coli-Inspector (Vischer). FM 4-64 membrane stain was employed to differentiate between cells that had completed division and those that had not. For analysis of cell cycle progression, cells were considered positive for FtsZ-ring formation if they contained a visible band or two spots of GFP-FtsZ fluorescence at midcell. Cells were also considered positive for FtsZ-ring formation if a single spot of GFP-FtsZ was visible at the midpoint of an invaginating septum.

Measurement of steady-state intracellular nucleotides by thin layer chromatography.

Strains were grown from single colonies in low-phosphate MOPS (Teknova) at 37°C with shaking (1X MOPS, 1 mM KH_2PO_4, 0.2% glucose, 0.4% casamino acids) and appropriate antibiotics to early logarithmic phase, then diluted to OD_{600} = 0.005, at which time ^{32}P-orthophosphate was introduced to label the cells. Once cells reached early logarithmic phase

again, samples were collected for nucleotide extraction using 2M ice cold formic acid. Nucleotides were measured using thin layer chromatography and quantified using ImageQuant software (Molecular Dynamics) as described previously (Wang et al., 2007). Intensities were normalized to the number of phosphates in the corresponding nucleotide. ppGpp levels are normalized to GTP level at steady state with signals from steady-state (p)ppGpp^0 cells subtracted.

Cell viability assays

Cells were grown in LB-0.2% glucose at 37°C from a single colony to OD_{600} = 0.2-0.3, back-diluted to OD_{600} = 0.005, and returned to 37°C with shaking. At OD_{600} ~ 0.4, cultures were divided equally and exposed to either 500 μg/ml cerulenin, an equal volume of 95% EtOH as a solvent control or left untreated. Serial dilutions of each sample were spread on LB agar every 30 minutes after treatment. Colony forming units (CFUs) were enumerated after 24 h of incubation at 37°C. Because ppGpp^0 cells tend to accumulate suppressor mutations in RNA polymerase, ppGpp^0 samples were plated on AB-minimal + 0.2% glucose and LB agar to identify suppressor mutants. The frequency of ppGpp^0 suppressor mutants was calculated as the ratio of CFU/ml recovered on minimal vs. LB plates. Data was only included from experiments where the ratio of CFU/ml recovered on minimal vs. LB plates was less than 1:10.

Assessment of cell envelope integrity via propidium iodide incorporation

Cells were grown in LB-0.2% glucose at 37°C from a single colony to OD_{600} = 0.2-0.3, back-diluted to OD_{600} = 0.005, and returned to 37°C. At OD_{600} ~ 0.4, cultures were divided equally and exposed to either 1.5 μM propidium iodide alone, or propidium iodide and either 500 μg/ml

cerulenin or an equal volume of 95% EtOH as a solvent control. At indicated intervals, samples were removed and mounted on 1% agarose pads for phase contrast and fluorescence imaging. The extent of propidium iodide incorporation was measured by quantitative fluorescence microscopy. Briefly, fluorescence images were background corrected, bacteria from phase contrast images were outlined as regions of interest (ROIs) and the average fluorescence intensity per cell of the ROIs was determined from background corrected fluorescence images.

Statistical analysis

A minimum of three independent biological replicates were performed for each experimental data set. Data were expressed as means ± standard errors of the means (SEM). *P* values were calculated using a standard two-tailed Student's *t* test. Asterisks indicate a significant difference between the results for indicated experimental conditions (*, $P < 0.05$; **, $P < 0.01$).

Author Contributions

S.V., P.A.L., J.D.W., and J.L.T. designed the experiments. S.V. and J.L.T. performed the experiments. P.A.L. and S.V. wrote the manuscript.

Acknowledgements

We are indebted to Mike Cashel, John Cronan, Christophe Herman, Rick Gourse, Charles Rock, and Fuzhong Zhang for the kind gift of *E. coli* strains and plasmids, and to Dianne Duncan, Norbert Vischer and Anne Katherine Fee for assistance with image capture and analysis. We would also like to thank Gayle Bentley, Natacha Ruiz and members of the Levin and Zaher labs for numerous discussions about matters technical and philosophical over the course of this research, and Heidi Arjes, Rick Gourse, Daniel Haeusser and Suckjoon Jun for critical reading of

575 the manuscript. This work was supported by National Institutes of Health grants GM64671 to
576 PAL and GM084003 to JDW.
577

578 ## References

579 Adams, D.W., and Errington, J. (2009). Bacterial cell division: assembly, maintenance and disassembly of the Z
580 ring. Nat Rev Microbiol *7*, 642-653.

581 Amir, A. (2014). Cell Size Regulation in Bacteria. Phys Rev Lett *112*.

582 Arjes, H.A., Kriel, A., Sorto, N.A., Shaw, J.T., Wang, J.D., and Levin, P.A. (2014). Failsafe mechanisms couple
583 division and DNA replication in bacteria. Curr Biol *24*, 2149-2155.

584 Arndt-Jovin, D.J., and Jovin, T.M. (1989). Fluorescence labeling and microscopy of DNA. Methods Cell Biol *30*,
585 417-448.

586 Basan, M., Hui, S., Okano, H., Zhang, Z., Shen, Y., Williamson, J.R., and Hwa, T. (2015a). Overflow metabolism in
587 Escherichia coli results from efficient proteome allocation. Nature *528*, 99-104.

588 Basan, M., Zhu, M., Dai, X., Warren, M., Sevin, D., Wang, Y.P., and Hwa, T. (2015b). Inflating bacterial cells by
589 increased protein synthesis. Mol Syst Biol *11*, 836.

590 Battesti, A., and Bouveret, E. (2006). Acyl carrier protein/SpoT interaction, the switch linking SpoT-dependent
591 stress response to fatty acid metabolism. Mol Microbiol *62*, 1048-1063.

592 Black, P.N., and DiRusso, C.C. (2003). Transmembrane movement of exogenous long-chain fatty acids: proteins,
593 enzymes, and vectorial esterification. Microbiol Mol Biol Rev *67*, 454-472, table of contents.

594 Bowman, A.M., Nesin, O.M., Pakhomova, O.N., and Pakhomov, A.G. (2010). Analysis of plasma membrane
595 integrity by fluorescent detection of Tl(+) uptake. J Membr Biol *236*, 15-26.

596 Burke, C., Liu, M., Britton, W., Triccas, J.A., Thomas, T., Smith, A.L., Allen, S., Salomon, R., and Harry, E.
597 (2013). Harnessing single cell sorting to identify cell division genes and regulators in bacteria. PLoS One *8*, e60964.

598 Cambridge, J., Blinkova, A., Magnan, D., Bates, D., and Walker, J.R. (2014). A replication-inhibited unsegregated
599 nucleoid at mid-cell blocks Z-ring formation and cell division independently of SOS and the SlmA nucleoid
600 occlusion protein in Escherichia coli. J Bacteriol *196*, 36-49.

601 Campos, M., Surovtsev, I.V., Kato, S., Paintdakhi, A., Beltran, B., Ebmeier, S.E., and Jacobs-Wagner, C. (2014). A
602 constant size extension drives bacterial cell size homeostasis. Cell *159*, 1433-1446.

603 Clark, J.D.a.M., O. (1967). DNA Replication and the Division Cycle in Escherichia coli. J Mol Biol *23*, 99-112.

604 Cooper, S. (1969). Cell division and DNA replication following a shift to a richer medium. J Mol Biol *43*, 1-11.

605 Cronan, J.E. (2014). A new pathway of exogenous fatty acid incorporation proceeds by a classical phosphoryl
606 transfer reaction. Mol Microbiol *92*, 217-221.
607 D'Ari, R., and Huisman, O. (1983). Novel mechanism of cell division inhibition associated with the SOS response in
608 Escherichia coli. J Bacteriol *156*, 243-250.
609 Davie, E., and Petersen, J. (2012). Environmental control of cell size at division. Curr Opin Cell Biol *24*, 838-844.
610 Davis, M.S., Solbiati, J., and Cronan, J.E., Jr. (2000). Overproduction of acetyl-CoA carboxylase activity increases
611 the rate of fatty acid biosynthesis in Escherichia coli. J Biol Chem *275*, 28593-28598.
612 den Blaauwen, T., Buddelmeijer, N., Aarsman, M.E., Hameete, C.M., and Nanninga, N. (1999). Timing of FtsZ
613 assembly in Escherichia coli. J Bacteriol *181*, 5167-5175.
614 Edgar, B.A. (2006). How flies get their size: genetics meets physiology. Nat Rev Genet *7*, 907-916.
615 Ferullo, D.J., and Lovett, S.T. (2008). The stringent response and cell cycle arrest in Escherichia coli. PLoS Genet *4*,
616 e1000300.
617 Fredborg, M., Rosenvinge, F.S., Spillum, E., Kroghsbo, S., Wang, M., and Sondergaard, T.E. (2015). Automated
618 image analysis for quantification of filamentous bacteria. BMC Microbiol *15*, 255.
619 Ginzberg, M.B., Kafri, R., and Kirschner, M. (2015). Cell biology. On being the right (cell) size. Science *348*,
620 1245075.
621 Golzio, M., Teissie, J., and Rols, M.P. (2002). Direct visualization at the single-cell level of electrically mediated
622 gene delivery. Proc Natl Acad Sci USA *99*, 1292-1297.
623 Hale, C.A., and de Boer, P.A. (1999). Recruitment of ZipA to the septal ring of Escherichia coli is dependent on
624 FtsZ and independent of FtsA. J Bacteriol *181*, 167-176.
625 Harris, L.K., and Theriot, J.A. (2016). Relative Rates of Surface and Volume Synthesis Set Bacterial Cell Size. Cell
626 *165*, 1479-1492.
627 Heath, R.J., Jackowski, S., and Rock, C.O. (1994). Guanosine tetraphosphate inhibition of fatty acid and
628 phospholipid synthesis in Escherichia coli is relieved by overexpression of glycerol-3-phosphate acyltransferase
629 (plsB). J Biol Chem *269*, 26584-26590.
630 Hill, N.S., Buske, P.J., Shi, Y., and Levin, P.A. (2013). A moonlighting enzyme links Escherichia coli cell size with
631 central metabolism. PLoS Genet *9*, e1003663.

632 Huisman, O., and D'Ari, R. (1981). An inducible DNA replication-cell division coupling mechanism in E. coli.
633 Nature *290*, 797-799.
634 Huisman, O., D'Ari, R., and Gottesman, S. (1984). Cell-division control in Escherichia coli: specific induction of the
635 SOS function SfiA protein is sufficient to block septation. Proc Natl Acad Sci USA *81*, 4490-4494.
636 Ishiguro, E.E., and Ramey, W.D. (1976). Stringent control of peptidoglycan biosynthesis in Escherichia coli K-12. J
637 Bacteriol *127*, 1119-1126.
638 Ishiguro, E.E., and Ramey, W.D. (1978). Involvement of the relA gene product and feedback inhibition in the
639 regulation of DUP-N-acetylmuramyl-peptide synthesis in Escherichia coli. J Bacteriol *135*, 766-774.
640 Iyer-Biswas, S., Wright, C.S., Henry, J.T., Lo, K., Burov, S., Lin, Y., Crooks, G.E., Crosson, S., Dinner, A.R., and
641 Scherer, N.F. (2014). Scaling laws governing stochastic growth and division of single bacterial cells. Proc Natl Acad
642 Sci USA *111*, 15912-15917.
643 Kellogg, D.R. (2003). Wee1-dependent mechanisms required for coordination of cell growth and cell division. J
644 Cell Sci *116*, 4883-4890.
645 Laplante, M., and Sabatini, D.M. (2009). An emerging role of mTOR in lipid biosynthesis. Curr Biol *19*, R1046-
646 1052.
647 Leslie, D.J., Heinen, C., Schramm, F.D., Thuring, M., Aakre, C.D., Murray, S.M., Laub, M.T., and Jonas, K. (2015).
648 Nutritional Control of DNA Replication Initiation through the Proteolysis and Regulated Translation of DnaA. PLoS
649 Genet *11*, e1005342.
650 Levin, P.A. (2002). Light microscopy techniques for bacterial cell biology. Methods Microbiol *31*, 115-132.
651 Li, S.J., and Cronan, J.E., Jr. (1993). Growth rate regulation of Escherichia coli acetyl coenzyme A carboxylase,
652 which catalyzes the first committed step of lipid biosynthesis. J Bacteriol *175*, 332-340.
653 Liu, K., Bittner, A.N., and Wang, J.D. (2015). Diversity in (p)ppGpp metabolism and effectors. Curr Opin Microbiol
654 *24*, 72-79.
655 Lobner-Olesen, A., Skarstad, K., Hansen, F.G., von Meyenburg, K., and Boye, E. (1989). The DnaA protein
656 determines the initiation mass of Escherichia coli K-12. Cell *57*, 881-889.
657 Loewith, R., and Hall, M.N. (2011). Target of rapamycin (TOR) in nutrient signaling and growth control. Genetics
658 *189*, 1177-1201.

659 Mercier, R., Kawai, Y., and Errington, J. (2013). Excess membrane synthesis drives a primitive mode of cell
660 proliferation. Cell *152*, 997-1007.
661 Murray, H.D., Appleman, J.A., and Gourse, R.L. (2003). Regulation of the Escherichia coli rrnB P2 promoter. J
662 Bacteriol *185*, 28-34.
663 My, L., Rekoske, B., Lemke, J.J., Viala, J.P., Gourse, R.L., and Bouveret, E. (2013). Transcription of the
664 Escherichia coli fatty acid synthesis operon fabHDG is directly activated by FadR and inhibited by ppGpp. J
665 Bacteriol *195*, 3784-3795.
666 Parsons, J.B., and Rock, C.O. (2013). Bacterial lipids: metabolism and membrane homeostasis. Prog Lipid Res *52*,
667 249-276.
668 Pierucci, O. (1978). Dimensions of Escherichia coli at various growth rates: model for envelope growth. J Bacteriol
669 *135*, 559-574.
670 Podkovyrov, S.M., and Larson, T.J. (1996). Identification of promoter and stringent regulation of transcription of the
671 fabH, fabD and fabG genes encoding fatty acid biosynthetic enzymes of Escherichia coli. Nucleic Acids Res *24*,
672 1747-1752.
673 Pritchard, R.H., Meacock, P.A., and Orr, E. (1978). Diameter of cells of a thermosensitive dnaA mutant of
674 Escherichia coli cultivated at intermediate temperatures. J Bacteriol *135*, 575-580.
675 Ross, W., Vrentas, C.E., Sanchez-Vazquez, P., Gaal, T., and Gourse, R.L. (2013). The magic spot: a ppGpp binding
676 site on E. coli RNA polymerase responsible for regulation of transcription initiation. Mol Cell *50*, 420-429.
677 Roth, V. (2006). http://www.doubling-time.com/compute_more.php.
678 Rowlett, V.W., and Margolin, W. (2015). The Min system and other nucleoid-independent regulators of Z ring
679 positioning. Front Microbiol *6*, 478.
680 Sargent, M.G. (1975). Control of cell length in Bacillus subtilis. J Bacteriol *123*, 7-19.
681 Sarubbi, E., Rudd, K.E., and Cashel, M. (1988). Basal ppGpp level adjustment shown by new spoT mutants affect
682 steady state growth rates and rrnA ribosomal promoter regulation in Escherichia coli. Molecular & general genetics :
683 MGG *213*, 214-222.
684 Schaechter, M., Maaloe, O., and Kjeldgaard, N.O. (1958). Dependency on medium and temperature of cell size and
685 chemical composition during balanced grown of Salmonella typhimurium. J Gen Microbiol *19*, 592-606.

686 Schreiber, G., Metzger, S., Aizenman, E., Roza, S., Cashel, M., and Glaser, G. (1991). Overexpression of the relA
687 gene in Escherichia coli. J Biol Chem *266*, 3760-3767.
688 Schreiber, G., Ron, E.Z., and Glaser, G. (1995). ppGpp-mediated regulation of DNA replication and cell division in
689 Escherichia coli. Curr Microbiol *30*, 27-32.
690 Seyfzadeh, M., Keener, J., and Nomura, M. (1993). spoT-dependent accumulation of guanosine tetraphosphate in
691 response to fatty acid starvation in Escherichia coli. Proc Natl Acad Sci USA *90*, 11004-11008.
692 Stott, K.V., Wood, S.M., Blair, J.A., Nguyen, B.T., Herrera, A., Mora, Y.G., Cuajungco, M.P., and Murray, S.R.
693 (2015). (p)ppGpp modulates cell size and the initiation of DNA replication in Caulobacter crescentus in response to
694 a block in lipid biosynthesis. Microbiology *161*, 553-564.
695 Svitil, A.L., Cashel, M., and Zyskind, J.W. (1993). Guanosine tetraphosphate inhibits protein synthesis in vivo. A
696 possible protective mechanism for starvation stress in Escherichia coli. J Biol Chem *268*, 2307-2311.
697 Taheri-Araghi, S., Bradde, S., Sauls, J.T., Hill, N.S., Levin, P.A., Paulsson, J., Vergassola, M., and Jun, S. (2015).
698 Cell-size control and homeostasis in bacteria. Curr Biol *25*, 385-391.
699 Tedin, K., and Bremer, H. (1992). Toxic effects of high levels of ppGpp in Escherichia coli are relieved by rpoB
700 mutations. J Biol Chem *267*, 2337-2344.
701 Tehranchi, A.K., Blankschien, M.D., Zhang, Y., Halliday, J.A., Srivatsan, A., Peng, J., Herman, C., and Wang, J.D.
702 (2010). The transcription factor DksA prevents conflicts between DNA replication and transcription machinery. Cell
703 *141*, 595-605.
704 Traxler, M.F., Summers, S.M., Nguyen, H.T., Zacharia, V.M., Hightower, G.A., Smith, J.T., and Conway, T.
705 (2008). The global, ppGpp-mediated stringent response to amino acid starvation in Escherichia coli. Mol Microbiol
706 *68*, 1128-1148.
707 Vischer, N. https://sils.fnwi.uva.nl/bcb/objectj/ (University of Amsterdam).
708 Vischer, N.O., Verheul, J., Postma, M., van den Berg van Saparoea, B., Galli, E., Natale, P., Gerdes, K., Luirink, J.,
709 Vollmer, W., Vicente, M., *et al.* (2015). Cell age dependent concentration of Escherichia coli divisome proteins
710 analyzed with ImageJ and ObjectJ. Front Microbiol *6*, 586.
711 Wallden, M., Fange, D., Lundius, E.G., Baltekin, O., and Elf, J. (2016). The Synchronization of Replication and
712 Division Cycles in Individual E. coli Cells. Cell *166*, 729-739.

713 Wang, J.D., Sanders, G.M., and Grossman, A.D. (2007). Nutritional control of elongation of DNA replication by
714 (p)ppGpp. Cell *128*, 865-875.
715 Weart, R.B., Lee, A.H., Chien, A.C., Haeusser, D.P., Hill, N.S., and Levin, P.A. (2007). A metabolic sensor
716 governing cell size in bacteria. Cell *130*, 335-347.
717 Weart, R.B., and Levin, P.A. (2003). Growth rate-dependent regulation of medial FtsZ ring formation. J Bacteriol
718 *185*, 2826-2834.
719 Wood, E., and Nurse, P. (2015). Sizing up to divide: mitotic cell-size control in fission yeast. Annu Rev Cell Dev
720 Biol *31*, 11-29.
721 Xiao, H., Kalman, M., Ikehara, K., Zemel, S., Glaser, G., and Cashel, M. (1991). Residual guanosine 3',5'-
722 bispyrophosphate synthetic activity of relA null mutants can be eliminated by spoT null mutations. J Biol Chem *266*,
723 5980-5990.
724 Yao, Z., Davis, R.M., Kishony, R., Kahne, D., and Ruiz, N. (2012a). Regulation of cell size in response to nutrient
725 availability by fatty acid biosynthesis in Escherichia coli. Proc Natl Acad Sci USA *109*, E2561-2568.
726 Yao, Z., Kahne, D., and Kishony, R. (2012b). Distinct single-cell morphological dynamics under beta-lactam
727 antibiotics. Mol Cell *48*, 705-712.
728 Young, K.D. (2010). Bacterial shape: two-dimensional questions and possibilities. Annu Rev Microbiol *64*, 223-
729 240.
730 Zhang, F., Ouellet, M., Batth, T.S., Adams, P.D., Petzold, C.J., Mukhopadhyay, A., and Keasling, J.D. (2012).
731 Enhancing fatty acid production by the expression of the regulatory transcription factor FadR. Metab Eng *14*, 653-
732 660.
733
734
735
736
737
738
739

740

741

742

743

744

745

Figure Legends

Figure 1. RNA, protein and fatty acid synthesis differentially impact cell size. (A) Plots of mass doublings/hour versus mean square area, mean length and mean width for cells cultured in different carbon sources, or cultured in LB-glc and treated with subinhibitory concentrations of antibiotics inhibiting RNA (rifampicin), protein (chloramphenicol), or fatty acid synthesis (cerulenin). (B) Plots of doubling time versus percent of cells with FtsZ rings for the above conditions. (C) Mass doublings/hour versus mean square area for cells with loss-of-function mutations in *fabH*, whose product catalyzes the conversion of acetyl-CoA and malonyl-acyl-carrier-protein to acetoacetyl-acyl-carrier-protein in one of the first steps in fatty acid synthesis. All data points indicate averages from n ≥3 experiments, ≥100 cells measured per experiment. Error bars = standard error of the mean (SEM). Black lines indicate the line of best fit of data from cells cultured in different carbon sources. Blue, green, red, and purple lines indicate lines of best fit for respective treatments. Wedges indicate increasing carbon availability or antibiotic concentration for respective conditions.

Figure 2. Protein-dependent changes in cell size are lipid-dependent. Cell size distributions following inhibition of fatty acid synthesis (A) or protein synthesis (B) in the presence or absence of exogenous oleic acid. Cer = 70 μg/ml cerulenin. Cm = 1.5 μg/ml chloramphenicol. OA = 10 μg/ml oleic acid. Distribution curves compiled from n ≥3 experiments for each condition, ≥100 cells measured in each experiment.

Figure 3. Cell size scales with lipid availability. (A) Overproduction of the transcriptional activator of fatty acid synthesis, FadR, increases cell size. Asterisks indicate a significant

769 difference compared to wild-type MG1655. * $p < 0.05$ by t-test. (B) Representative phase
770 contrast images of *E. coli* MG1655 or MG1655-*pFadR*. Scale bar = 5 μm. (C) Cell size
771 histogram showing cell size distribution versus induction of *pFadR*. (D) Plot of cell size versus
772 growth rate following induction of *pFadR*. Black line indicates best fit data from MG1655
773 cultured in different carbon sources (reproduced from Figure 1C). Red line indicates best fit data
774 for MG1655-*pFadR*. Means are compiled from n ≥3 experiments for each condition, ≥ 100 cells
775 measured in each experiment. Error bars = SEM. Color key indicates different IPTG
776 concentrations and applies to panels A, C and D.
777
778 **Figure 4. Lipid synthesis and nutrient availability impact size independent of ppGpp.** (A)
779 Histogram of cells engineered to overproduce the ppGpp synthase RelA alone and in
780 combination with the transcriptional activator FadR in response to 10 μM IPTG (B) Plot of cell
781 size versus growth rate of wild-type MG1655 and $ppGpp^0$ strains cultured in different carbon
782 sources: LB-glc, LB, AB-caa-glc, AB-caa-succ, for both strains as well as AB-glc and AB-succ
783 for the wild-type strain. (The $ppGpp^0$ strain cannot grow without the addition of casamino acids).
784 Black and grey lines indicate lines of best fit for wild-type and $ppGpp^0$ data sets, respectively.
785 Compiled from n ≥3 experiments for each condition, ≥100 cells measured in each experiment.
786 Error bars = SEM.
787
788 **Figure 5. ppGpp is required to preserve membrane integrity and cell viability in the**
789 **absence of fatty acid synthesis** (A) Colony forming units versus time for wild-type MG1655
790 and $ppGpp^0$ strains. Cells were grown to OD_{600} of ~0.4 in LB-glc, treated with 500 μg/ml of
791 cerulenin (at t = 0) and plated on LB agar every 30 min following cerulenin addition for 240 min.

(B) Mean fluorescence intensity versus time of wild-type and $ppGpp^0$ cells treated with cerulenin in the presence of the nucleic acid stain propridium iodide (diameter >2nm) which is unable to efficiently cross intact cellular membranes. (C) Images of cells sampled at selected time points from (B). Intense fluorescence is indicative of loss of membrane integrity. Scale bar = 2μm.

Figure 6. Plasma membrane capacity is coupled to cell volume via the alarmone ppGpp. During growth in nutrient rich medium, carbon-dependent flux (dark blue arrows) through fatty acid synthesis is high, increasing the pool of lipids available for cell envelope synthesis and with it cell size. In nutrient poor medium, flux through lipid synthesis is curtailed, reducing membrane capacity and cell volume. Synthesis of cytoplasmic material (e.g. RNA, protein) is similarly dependent on nutrient availability. RNA and protein synthesis impact synthesis of fatty acids and lipids indirectly (light blue arrows) via production of key enzymes. Lipid synthesis is coupled to synthesis of cytoplasmic material via the alarmone ppGpp (red lines).

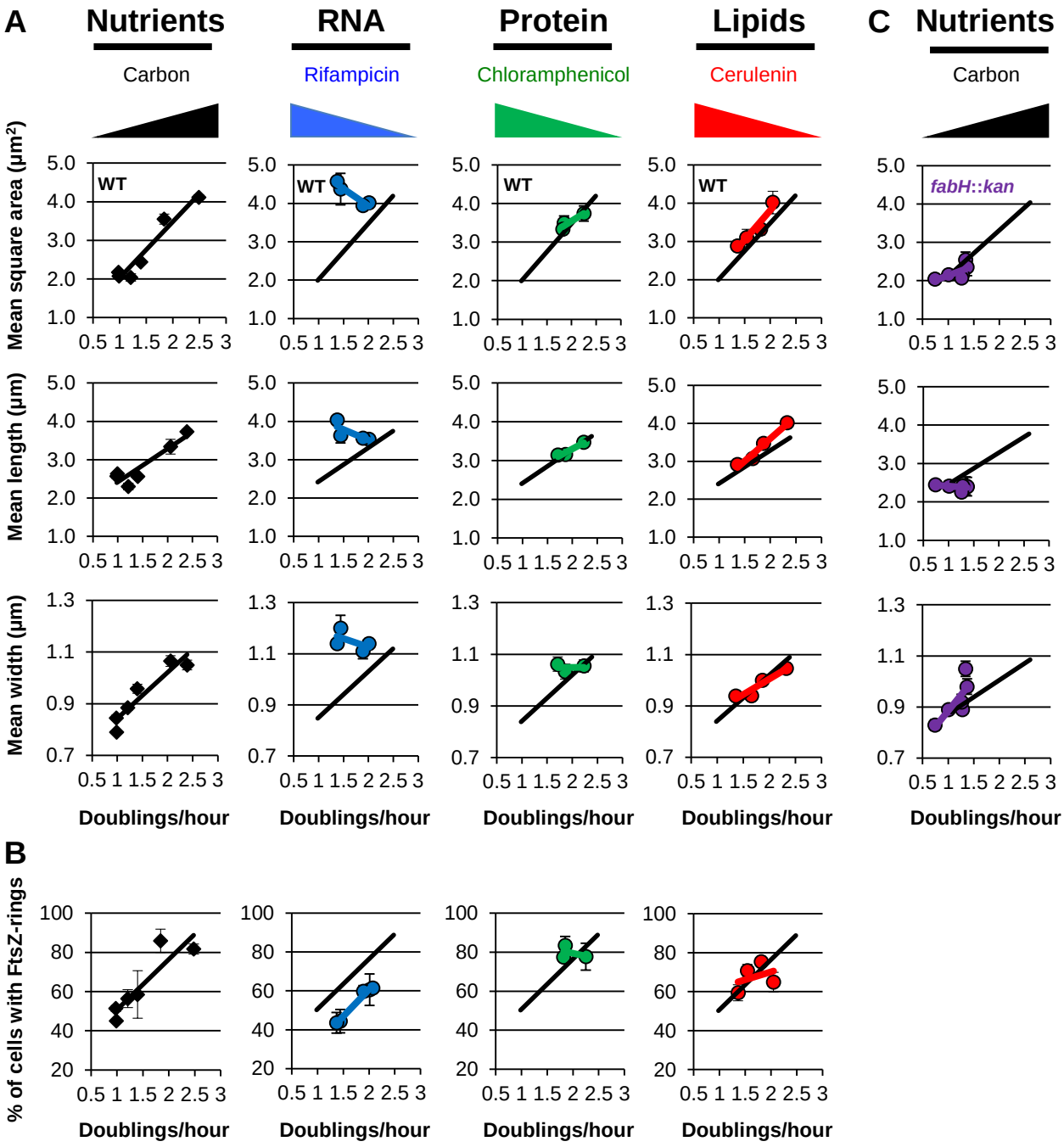

Figure 1

A

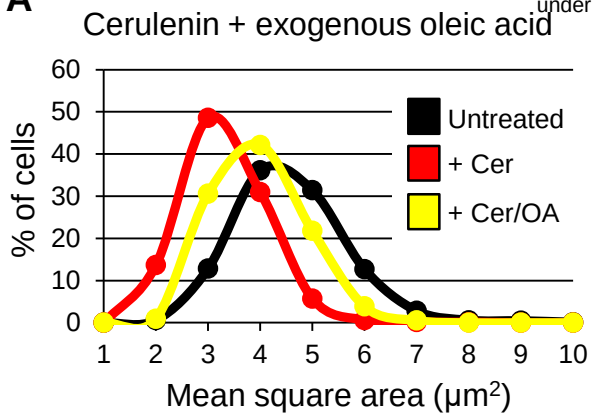

B

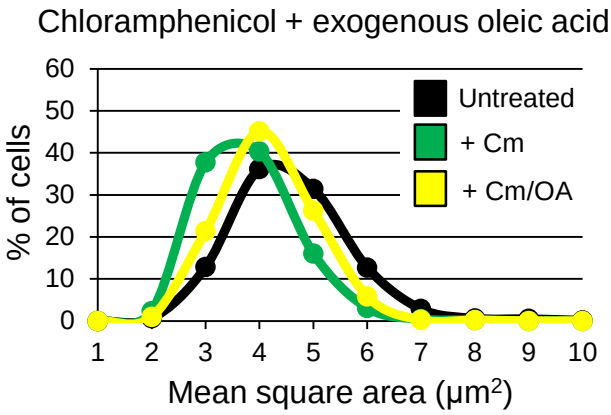

Figure 2

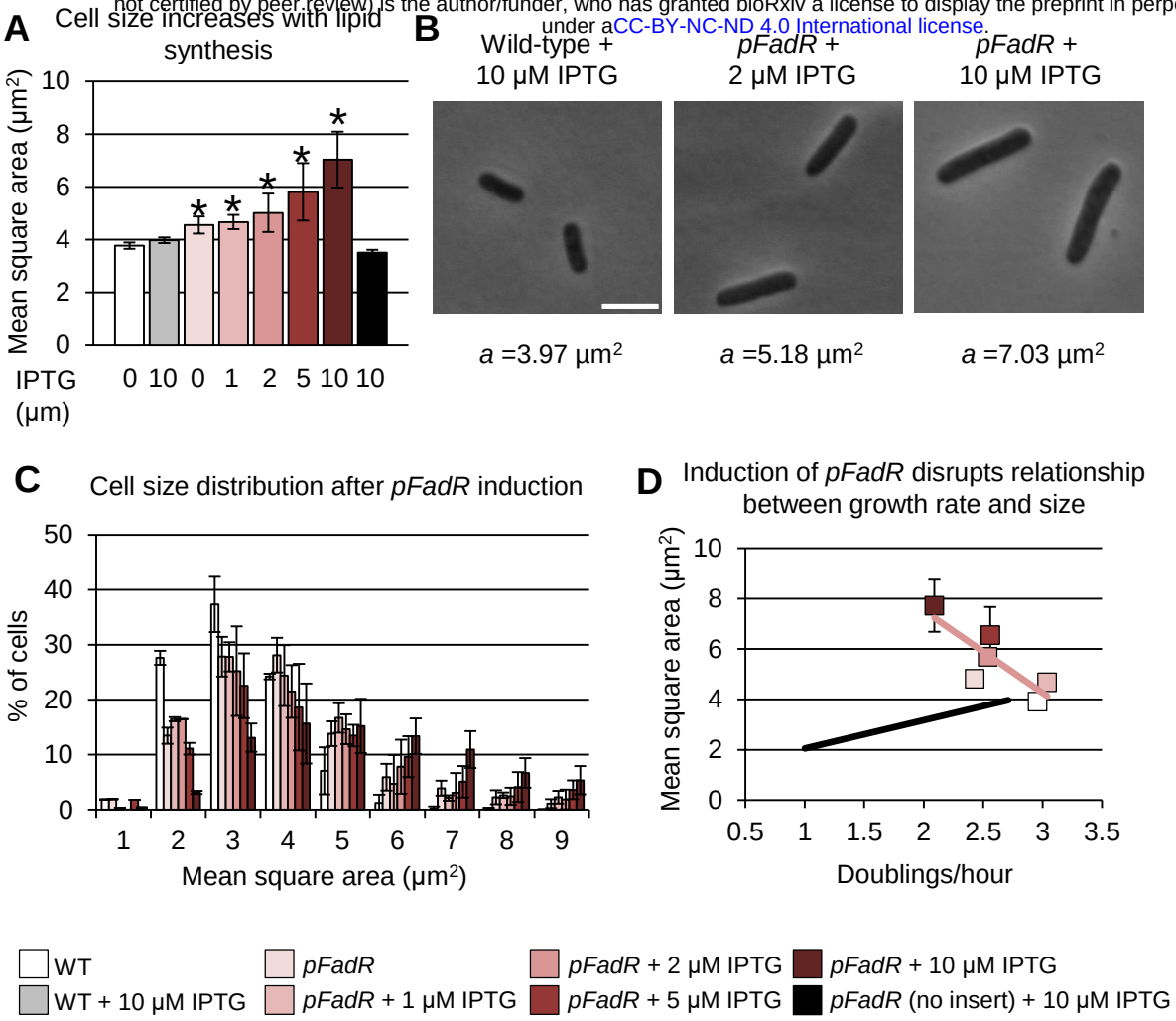

Figure 3

A

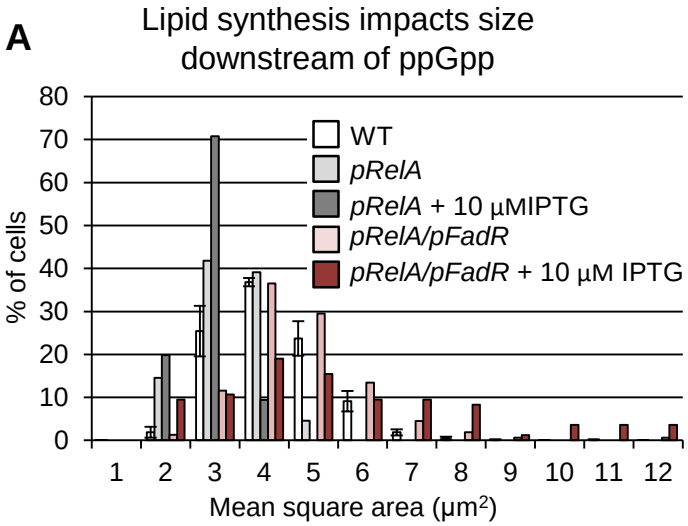

B

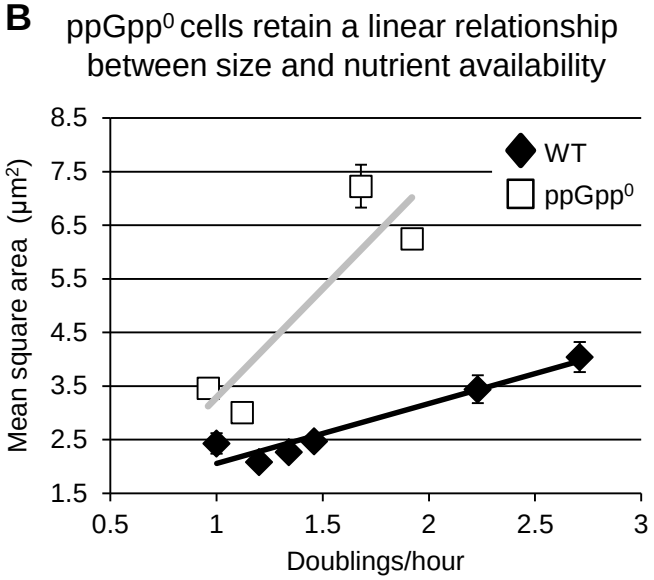

Figure 4

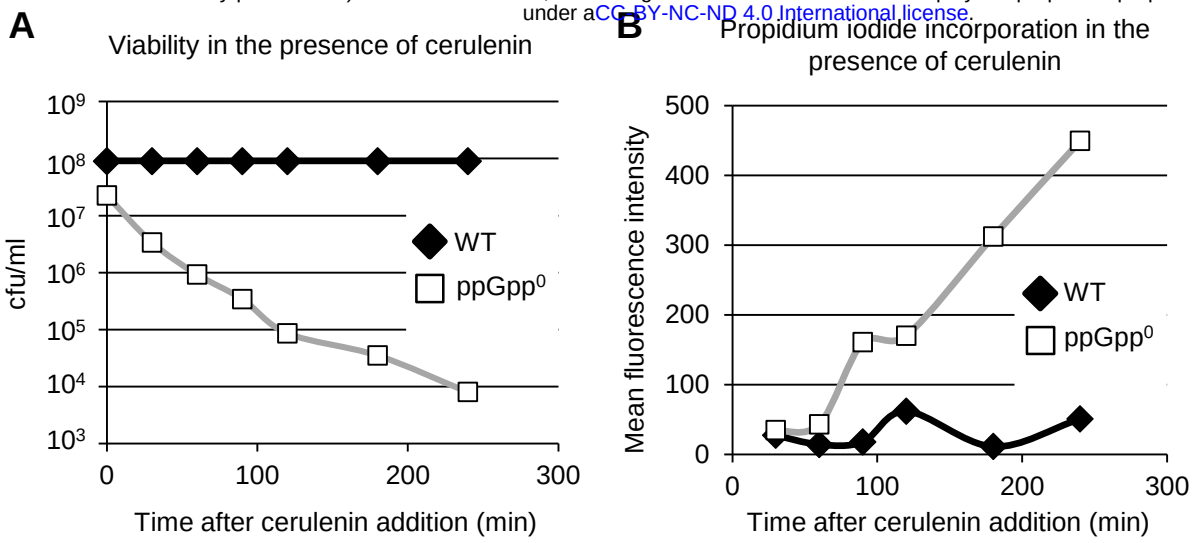

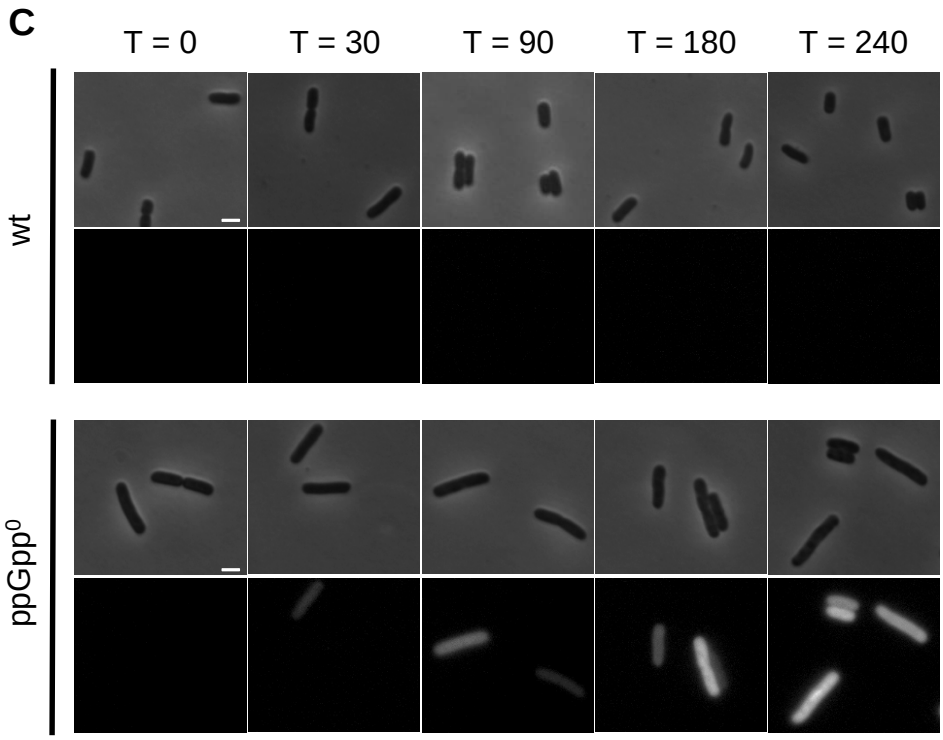

Figure 5

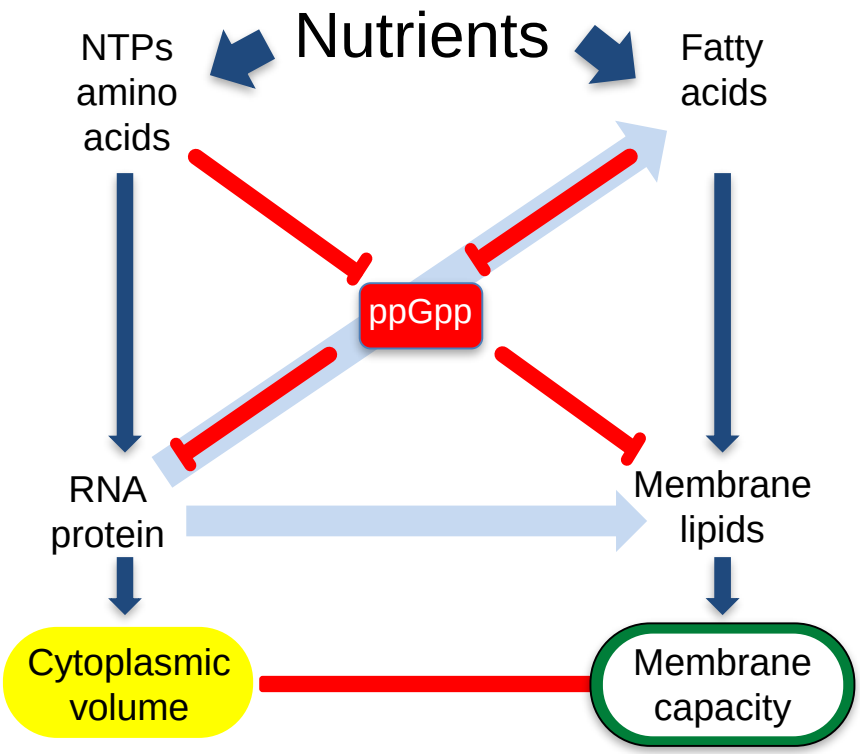

Figure 6